



HAL
open science

Radiation induced segregation near dislocations and symmetric tilt grain boundaries in Fe-Cr alloys: A phase-field study

Gabriel-Franck Bouobda Moladje, Ludovic Thuinet, Charlotte Becquart, Alexandre Legris

► **To cite this version:**

Gabriel-Franck Bouobda Moladje, Ludovic Thuinet, Charlotte Becquart, Alexandre Legris. Radiation induced segregation near dislocations and symmetric tilt grain boundaries in Fe-Cr alloys: A phase-field study. *Acta Materialia*, 2022, *Acta Materialia*, 225, pp.117523. 10.1016/j.actamat.2021.117523 . hal-03879757

HAL Id: hal-03879757

<https://hal.univ-lille.fr/hal-03879757>

Submitted on 8 Jan 2024

HAL is a multi-disciplinary open access archive for the deposit and dissemination of scientific research documents, whether they are published or not. The documents may come from teaching and research institutions in France or abroad, or from public or private research centers.

L'archive ouverte pluridisciplinaire **HAL**, est destinée au dépôt et à la diffusion de documents scientifiques de niveau recherche, publiés ou non, émanant des établissements d'enseignement et de recherche français ou étrangers, des laboratoires publics ou privés.



Distributed under a Creative Commons Attribution - NonCommercial 4.0 International License

Radiation induced segregation near dislocations and symmetric tilt grain boundaries in Fe-Cr alloys: a phase-field study

G.F. Bouobda Moladje^a, L. Thuinet^{a,b,*}, C.S. Becquart^{a,b}, A. Legris^{a,b}

^a*Univ. Lille, CNRS, INRAE, Centrale Lille, UMR 8207 - UMET - Unité Matériaux et Transformations, F-59000 Lille, France*

^b*Laboratoire commun EDF-CNRS Étude et Modélisation des Microstructures pour le Vieillissement des matériaux (EM2VM), France*

Abstract

A phase-field model dedicated to dislocation climb under irradiation has been coupled to point defects and chemical species transport equations. It allows to predict radiation induced segregation in Fe-Cr alloys around dislocations in the isolated or stacking configuration like in symmetric tilt grain boundaries. This work is challenging for several reasons: (i) radiation induced segregation in Fe-Cr is difficult to simulate since Cr depletion or enrichment can occur, depending on the Cr nominal composition and temperature, (ii) dislocations are biased sinks due to their elastic fields which can not be ignored in this case and (iii) other surrounding microstructural defects can interact with dislocations and impact point defect and solute transport. To overcome (iii), a mean-field approach is adopted, in which the influence of the surrounding sinks is taken into account through the introduction of an over-

*Corresponding author: Tel: +33 (0) 320 33 62 25 / Fax: +33 (0) 320 43 65 91, e-mail: Ludovic.Thuinet@univ-lille.fr

Email address: Ludovic.Thuinet@univ-lille.fr (L. Thuinet)

all and uniform sink strength in the point defect diffusion equations. Despite the numerous parameters of the model, unknown experimental information and approximations made to make the simulations tractable, the numerical results are in good agreement with the experimental ones. Moreover, the model allows to identify the main physical parameters to correctly quantify radiation induced segregation in the case of dislocations. Among them, the point defect relaxation volumes are of first importance in comparison with the solute relaxation volume or the nature of the slip system.

Keywords: Phase-field modeling, Irradiated metals, Edge dislocation, Segregation, Elastic properties

1. Introduction

Radiation induced segregation (RIS) is a common phenomenon in irradiated materials and plays an important role on their microstructural evolution. The mobile point defects (PDs) produced under irradiation migrate towards sinks such as dislocations, dislocation loops and grain boundaries (GBs) which therefore accumulate the atomic species preferentially driven by PDs [1, 2]. In more details, the depletion or enrichment of each element in the vicinity of sinks occurs according to its relative interaction with the PD fluxes. RIS can be modeled in the framework of the thermodynamics of irreversible processes [3], in which the Onsager coefficients L_{ij} are key parameters to explain the kinetic response of an alloy subjected to thermodynamic forces and to obtain the fluxes of atoms towards sinks. They depend on temperature, stress fields, and local PD and solute concentrations. They can be determined in principle from diffusion experiments but for multicompo-

ment and concentrated alloys it is quite difficult to measure them [2]. For this reason, theoretical models have been developed to determine the Onsager matrix. Among them, the self-consistent mean-field (SCMF) model [4, 5, 6] has been extensively used and generalized to any periodic crystal structure thanks to the KINECLUE code [7]. Based on solute-PD binding and migration energies obtained with DFT, matrices have been computed in bcc [8, 9] and fcc alloys [10]. In atomistic kinetic Monte Carlo (AKMC) simulations, the Onsager coefficients can be calculated using the generalized Einstein equations [11, 12].

RIS profiles can also be obtained directly by AKMC simulations, in which PD jumps are described individually [13, 14, 15, 16]. However, this type of simulations is time consuming and limited to nanoscale systems [2]. Thus, to simulate larger systems, it is necessary to rest on continuous descriptions. The phase-field (PF) method is particularly adapted to study RIS because diffusion processes are naturally incorporated and moreover elastic interactions can be properly described [17], which is not the case yet in the AKMC method. The PF approach has been used by Piochaud et al. [18] to model RIS near a GB assimilated to a planar sink with no elastic interactions in Fe-Cr alloys. In [18], the kinetic equations used in the PF model to simulate RIS are based on the Onsager formalism. The Onsager transport coefficients L_{ij} and the driving force parameters (equilibrium PD concentrations, thermodynamic factors) were computed at the atomic scale using AKMC simulations fitted on DFT calculations. Piochaud et al. compared the predictions obtained by the PF method and the AKMC simulations, and found a good agreement for large ranges of compositions and temperatures investigated.

They also showed that a quantitative PF prediction of RIS requires a precise parameterization of the Onsager coefficients, equilibrium PD concentrations and thermodynamic factors. More recently, Thuinet et al. [19] used the kinetic parameterization of [18] to investigate RIS near a dipole of edge dislocations mimicking an interstitial dislocation loop. The results showed that without taking into account elastic interactions between PDs and dislocations, the tendency and the level of segregation near the dislocation cores are comparable to the ones obtained at a planar sink. However, with the elastic interactions, the segregation tendency and level around the cores change strongly. In particular, the criteria established for RIS prediction near neutral sinks based only on kinetic arguments [1, 2] must be reconsidered for biased sinks like dislocations. Li and Trinkle [20] studied the modification of the Si segregation near an edge dislocation due to its strain field via the vacancy diffusion in Ni under irradiation using a mesoscopic approach. They showed that Si atoms segregate in the compression region of the dislocation core despite the fact that Si is an oversize solute in Ni. In these studies [19, 20], dislocations act as perfect sinks and are assumed to be static which is a questionable assumption. This hypothesis is justified if the kinetics related to PD and atom diffusion is much larger than the dislocation climb velocity. It is the case for PDs in most of the cases, but it is not always verified for atoms.

The aim of this paper is to investigate RIS in Fe-Cr alloys near edge dislocations as well as in the neighborhood of low angle symmetric tilt grain boundaries (STGBs) by the PF method. Indeed, if a lot of works dedicated to RIS modeling at neutral sinks already exist in Fe-Cr alloys, it must be

emphasized that similar studies at biased sinks are scarce but required to reach a deep understanding of RIS establishment in that case, which is still lacking. In comparison to previous approaches [18, 19], the model developed in [21] has the advantage to allow for dislocation climb during RIS and is used in this work. The choice of this family of alloys is justified by their interest for the nuclear industry [22]. Indeed, ferritic steels enriched in Cr have a good creep and corrosion resistance. Furthermore, detailed experimental investigations of RIS on dislocations and STGBs have been performed using atom probe tomography (APT) on these alloys [23]. However, this work is quite challenging for several reasons. Firstly, the experimental results on RIS in ferritic steels are complicated to explain since, as illustrated by the review performed in [24] of very different materials and conditions, both Cr depletions and enrichments in the vicinity of sinks are observed, depending on temperature and Cr composition. Other factors, like the grain boundary misorientation, may also affect Cr segregation at sinks [25, 26]. The most recent theoretical studies [27, 28, 18] explain this diversity of Cr behaviors by a subtle balance between the enrichment due to self-interstitial atoms (SIAs) and the depletion due to vacancies, which originates from the small migration barrier for the Cr–vacancy exchange in Fe and from the absence of drag effect by vacancies. Ferritic alloys are therefore more complicated to simulate than austenitic alloys for which vacancies and interstitials both contribute to depletion of Cr and enrichment of Ni [2]. Secondly, the long-range elastic interactions between sinks, solute atoms and PDs, often ignored in RIS studies at grain boundaries, cannot be reasonably neglected in the case of dislocations. The main objectives and originalities of this paper are then

(i) to assess the PF capability to predict RIS near biased sinks by a precise comparison with the available experimental data and (ii) to numerically quantify the climb and elastic contributions to the establishment of the RIS profiles. Moreover, to the author’s knowledge, this paper reports the first attempt to model RIS at STGBs taking into account the climb process.

The assumptions and equations of the model are described in Section 2. The sinks, dislocations and STGBs, are explicitly described and allowed to migrate due to the absorption of PDs. They are embedded in an absorbing mean-field medium characterized by an overall sink strength. In Sections 3 and 4, the results of the model are compared with experiments and the influence of several physical parameters on RIS is presented and analyzed, allowing to discuss the relevance and limitations of the model in Section 5.

2. Methodology

In this paper, we want to simulate RIS at dislocations and low angle STGBs. In the first case, one dipole of dislocations is introduced in the PF computational domain, as represented in Fig. 1-a). In the second case, we use the Read and Shockley description [29], in which a STGB with the misorientation angle θ is described as an array of edge dislocations, separated by a distance h given by:

$$h = \frac{b}{2 \sin(\theta/2)} \simeq \frac{b}{\theta} \quad (1)$$

where b is the length of the Burgers vector. As a consequence, a pile-up of dipoles is introduced in the simulation domain in order to simulate STGBs, as shown in Fig. 1-b). The simulation domain is 2D, the number of PF cells

of size a_0 being respectively $N1$ and $N2$ along the directions \mathbf{e}_1 and \mathbf{e}_2 in Fig. 1. Note that there are several possibilities to describe a pile-up of edge dislocations in PF models depending on the elementary dipole used. In the following, the habit plane of the dipole is defined as the plane containing the two dislocations lines and its normal is labeled \mathbf{n} . One way to create a dipole of dislocations is to define an order parameter η^l equal to 1 in the portion of the plane between the two dislocation lines and 0 outside and to associate to this order parameter an eigenstrain equal to:

$$\varepsilon_{ij}^{0,\eta^l} = \frac{b_i n_j + b_j n_i}{2a_0} \quad (2)$$

where b_i and n_j are respectively the i^{th} component of the Burgers vector and the j^{th} component of the unit vector normal to the habit plane of the dipole. The elementary dipole can be such that: (i) \mathbf{n} parallel to \mathbf{b} (see Fig. 1-b)) or (ii) \mathbf{n} perpendicular to \mathbf{b} (see Fig. 1-b) of [30] for instance). In PF models for dislocations, the core corresponds to the region inside the habit plane of the dipole where the profile of η^l presents a diffuse gradient, going from 0 to 1. The motion of the dislocation is only allowed in this plane. Then, only climb (respectively glide) motion will be possible in case (i) (respectively (ii)). Up to now, most of the PF models for dislocations were dedicated to glide and then configuration (ii) was preferentially used. However, in this work, dislocation climb is under interest which requires the choice of configuration (i). The choice made in this work allows then to satisfy the conditions of [29] and at the same time to address the climb of the dislocations in the STGB as they absorb PDs.

To properly describe the PF model for a binary $A - B$ alloy used in

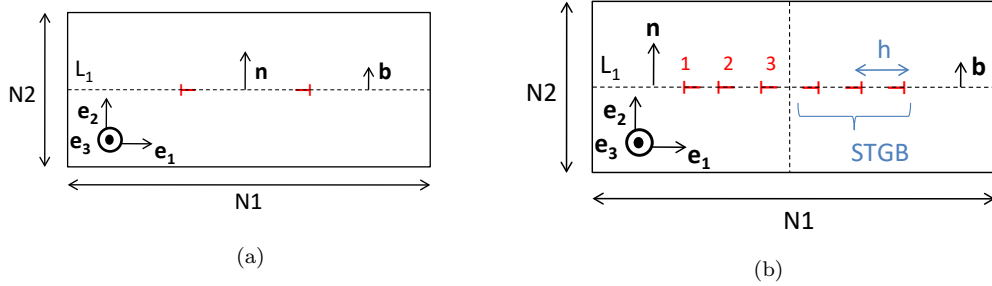


Figure 1: Simulation box (2D) containing a) a dipole of edge dislocations, b) a pile-up of edge dislocation dipoles or equivalently a low angle STGB. L_1 stands for the axis of the dislocation dipoles, i.e. the line passing through the cores of all dislocations.

this paper, the order parameters, total free energy of the system and evolution equations are successively presented. To simulate the diffusional flux couplings between PDs and chemical species, we need to introduce as order parameters the atomic fractions of vacancies X_V and SIAs X_I , as well as the atomic fractions X_A and X_B of the chemical species A and B (B being the solute). Since we want to simulate RIS at dislocations cores, it is also required to reproduce the sink behavior of the dislocations. This can be done by using the supplemental order parameters η_V^l and η_I^l which are related respectively to the atomic fraction of vacancies and SIAs absorbed or emitted by the dislocations. It can be easily shown that there is a relation between η_V^l , η_I^l and the classical order parameter η^l used in PF methods to represent a dislocation loop ($\eta^l = 1$ in the interior of the loop and 0 outside) since the dislocation loop grows or shrinks through the net absorption/emission of SIAs or vacancies according to its type (interstitial/vacancy):

$$\eta^l = \frac{1}{X^*} \text{sign}(l) (\eta_I^l - \eta_V^l) \quad (3)$$

$\text{sign}(l) = 1$ for interstitial loop and -1 for vacancy loop, $X^* = a_0/b$ is the

number of PDs required for a unitary climb process.

The total free energy of the system F is the sum of the chemical energy F_{ch} , dislocation core energy F_{core} and elastic energy F_{el} , which includes all the long-range interactions between the order parameters. The chemical free energy is given by:

$$F_{\text{ch}}(X_\alpha, X_d) = \frac{k_B T}{V_{\text{at}}} \left[\sum_\alpha \int_V X_\alpha \ln(\gamma_\alpha X_\alpha) dV + \sum_d \int_V X_d \ln\left(\frac{X_d}{X_d^{\text{eq}}}\right) dV \right] \quad (4)$$

where α stands for chemical species A and B , γ_α is the activity coefficient of alloying element α , V_{at} the atomic volume, V the total volume of the domain, k_B the Boltzmann constant, T the temperature of the system, and X_d^{eq} the PD atomic fraction at thermal equilibrium, d standing for vacancies or interstitials. In PF methods, the dislocation core energy is classically described as the sum of a crystalline and a gradient energy term and we suppose it only depends on η^l :

$$F_{\text{core}}(\eta^l) = F_{\text{cry}} + F_{\text{grad}} = \int_V [f_{\text{cry}}(\eta^l) + \frac{\gamma}{2} |\mathbf{n} \wedge \nabla \eta^l|^2] dV \quad (5)$$

with \mathbf{n} the normal to the habit plane of the loop. The gradient of η^l is projected on the habit plane of the loop to eliminate any energy contribution along \mathbf{n} . A simple double-well function is used for the crystalline energy [31, 32, 33] when only one dislocation dipole is considered like in Fig. 1-a):

$$f_{\text{cry}}^{\text{DW}}(\eta^l) = H(\eta^l)^2(1 - \eta^l)^2 \quad (6)$$

The coefficients H and γ control the dislocation core energy E_{core} and width w through the following expressions:

$$w = \sqrt{\frac{8\gamma}{H}}, \quad E_{\text{core}} = b\sqrt{\frac{H\gamma}{12}} \quad (7)$$

The crystalline energy given by a double-well potential does not allow to simulate several loops (parameter η^l can not have integer values superior to 1). In order to include in the proposed formalism these configurations like in STGBs of Fig. 1-b), we replace the double-well potential by a periodic function of η^l for which the minimum of the energy is reached for integer values of η^l :

$$f_{\text{cry}}^{\text{STGB}}(\eta^l) = (0.5)^4 \times H \sin^2(\pi \eta^l) \quad (8)$$

The elastic energy is calculated via the microelasticity theory [34] and is a function of the elastic strain which is the difference between the total strain $\varepsilon_{ij}(\mathbf{r})$ and the total eigenstrain $\varepsilon_{ij}^{0,\text{tot}}(\mathbf{r})$:

$$F_{\text{el}} = \frac{1}{2} \int_V C_{ijkl} [\varepsilon_{ij}(\mathbf{r}) - \varepsilon_{ij}^{0,\text{tot}}(\mathbf{r})] [\varepsilon_{kl}(\mathbf{r}) - \varepsilon_{kl}^{0,\text{tot}}(\mathbf{r})] dV \quad (9)$$

where C_{ijkl} are the elastic constants of the system. The total eigenstrain $\varepsilon_{ij}^{0,\text{tot}}$ depends on the PD and solute relaxation volumes Ω_d and Ω_B , as well as the Burgers vector \mathbf{b} and unit vector normal to the plane of the loop or the dipole \mathbf{n} , as shown by Eq. 2 [30, 21]. The total strain $\varepsilon_{ij}(\mathbf{r})$ is solved in the Fourier space, as detailed in [34, 35, 36, 37, 38].

The generation of PDs due to irradiation and the recombination between vacancies and interstitials are reproduced by adding respectively the terms K_0^d and J_R in the evolution equation of X_d . The recombination rate between vacancies and interstitials J_R can be derived from Waite's theory of the kinetics of diffusion-limited reactions [39]:

$$J_R = 4\pi d_{\text{rec}} \frac{D^i + D^v}{V_{\text{at}}} X_i X_v \quad (10)$$

with d_{rec} the recombination distance between PDs and D^d the diffusion coefficient of PD d . To simulate the presence of other sinks in the system (dislocation forest, grain boundaries, precipitates, ...), we introduce in the PD diffusion equation an additional absorption term $J_{s,d}^{\text{abs}}$:

$$J_{s,d}^{\text{abs}} = k_{s,d}^2 D^d (\bar{X}_d - X_d^s) \quad (11)$$

where $k_{s,d}^2$ is the overall sink strength of the surrounding microstructure for defect d , \bar{X}_d is the average value of X_d , X_d^s is the composition at the sink surface taken equal to X_d^{eq} . In other words, the presence of other sinks than the dislocation dipoles is represented by a mean field in each point of the domain to which the sink strength $k_{s,d}^2$ is associated.

In a binary $A - B$ alloy containing dislocations which can climb due to the absorption of SIAs and vacancies created by irradiation, it has been demonstrated that the evolution equations of the order parameters are given by [21]:

$$\frac{\partial X_d}{\partial t} = \nabla \cdot \left[\sum_{\alpha} \sum_{\beta} \frac{l_{\alpha\beta}^d X_d}{k_B T} (\text{sign}(d) \nabla \mu^{\beta} + \nabla \mu^d) \right] - \frac{\partial \eta_d^l}{\partial t} - J_{s,d}^{\text{abs}} - J_R + K_0^d \quad (12)$$

$$\frac{\partial \eta_d^l}{\partial t} = -L_{\eta^l}^d \left[\frac{1}{X^*} \text{sign}(l) \text{sign}(d) \mu^{\eta^l} - \mu^d \right] \quad (13)$$

$$\frac{\partial X_{\alpha}}{\partial t} = \nabla \cdot \left[\sum_d \sum_{\beta} \frac{l_{\alpha\beta}^d X_d}{k_B T} (\nabla \mu^{\beta} + \text{sign}(d) \nabla \mu^d) \right] \quad (14)$$

$\text{sign}(d) = -1$ for vacancies and $\text{sign}(d) = 1$ for interstitials. $l_{\alpha\beta}^d$ are the coefficients of the normalised Onsager matrix, where the subscripts α and β stand for A or B :

$$l_{\alpha\beta}^d = \frac{V_{\text{at}} k_B T}{X_d} L_{\alpha\beta}^d \quad (15)$$

Eq. 12 gives the temporal evolution of the PD atomic fraction field X_d :

- The first term on its right-hand side corresponds to the contribution of the PD fluxes which are coupled to the chemical fluxes and then depend on the PD potential μ^d ($\mu^d = V_{\text{at}} \frac{\delta F}{\delta X_d}$) but also on the potential of the chemical species μ^β ($\mu^\beta = V_{\text{at}} \frac{\delta F}{\delta X_\beta}$).

- The second term is the PD absorption term associated to the dislocations which behave like sinks for PDs.

- The third term is the PD absorption term by the other sinks present in the computational domain and represented by the overall sink strength $k_{s,d}^2$.

- **The fourth term stands for the annihilation of PDs due to recombination.**

- The last term is the PD irradiation source term.

Eq. 13 gives the evolution equation of the PD absorption term of the dislocations, and also allows to simulate the climb process which results from two antagonist effects appearing in the right-hand side: the first one is related to the driving forces due to the core and elastic energy of the loop μ^{η^l} ($\mu^{\eta^l} = V_{\text{at}} \frac{\delta F}{\delta \eta^l}$), whereas the second one is the osmotic force related to the PD supersaturation in the matrix. $L_{\eta^l}^d$ is a coefficient which controls the kinetics of PD absorption/emission by the dislocation cores and is related to the dislocation jog density, high values of this coefficient corresponding to the perfect sink behavior.

Finally, Eq. 14 is the evolution equation of the chemical species which can diffuse by vacancy and interstitial mechanisms.

3. Results

3.1. Definition of the reference case

In this paper, RIS is studied near straight edge dislocations and STGBs in Fe-Cr alloys with a nominal Cr atomic fraction $X_{\text{Cr}}^{\text{nom}}$ of 5% at 600 K. The thermodynamic and kinetic parameters, namely the PD thermal equilibrium fraction X_d^{eq} , the Onsager coefficients $L_{\alpha\beta}^d$ and the activity coefficients γ_α available in [18] are used. They have been determined from Monte Carlo simulations based on the model and parameters of [28]. The calculation of point defects jump frequencies is based on a rigid lattice broken-bond model using effective pair interactions depending on the temperature and local concentrations in order to properly take into account magnetic and vibrational contributions particularly significant in Fe-Cr alloys [40, 41]. Equilibrium PD concentrations X_d^{eq} are determined by the AKMC method presented in [42]. AKMC simulations are also used to calculate the coefficients $L_{\alpha\beta}^d$: one vacancy (respectively one interstitial) is introduced in a simulation box in which sites are either occupied by Fe or Cr atoms except one site representing a PD. During the Monte Carlo run, the statistical average of vector displacements of atoms α mediated by the PD is calculated and $L_{\alpha\beta}^d$ coefficients are then deduced using the generalized Einstein relations [43]. The variation of the alloy chemical potential (or equivalently the activity coefficients γ_α) is computed by performing Monte Carlo Metropolis (MCM) simulations combined with a Widom integration [44]. The main results concerning the dependence of all the thermodynamic and kinetic parameters on the temperature and local Cr concentration can be summarized as follows. X_d^{eq} are found to slightly depend on the composition, which is not the case for the alloy chemical potential: the lower the temperature, the greater is

its variation with composition. Based on the obtained values of $L_{\alpha\beta}^d$ and analytical diffusion models valid in simple cases (no precipitation, transport coefficients independent of the local composition, no mechanical stress, neutral sinks), it is shown that the vacancy contribution, leading to Cr depletion near PD sinks, is dominant only at high temperatures: above 900 K, Cr is expected to deplete near neutral sink on the whole composition range 0-20% at. Cr whereas at lower temperatures, there is a composition range on which Cr is expected to enrich, this composition range increasing with decreasing temperatures. It was already shown in the case of planar sinks that taking into account this variation of the thermodynamic and kinetic coefficients with local composition was required to quantitatively predict RIS [18]. As a consequence, these quantities are not taken constant and uniform at the nominal composition of the alloy but depend on the local composition in our simulations.

The other necessary parameters for the simulations are given in Table 1. The PD relaxation volumes are taken from [45] ($\Omega_1^{\text{ref}} = 1.08V_{\text{at}}$, $\Omega_{\text{V}}^{\text{ref}} = -0.048V_{\text{at}}$). The relaxation volume of Cr are set at zero ($\Omega_{\text{Cr}} = 0$) which is **equivalent to ignoring** the difference between the lattice parameters of Fe and Cr. **The kinetic coefficients $L_{\eta^i}^d$ are chosen such that the perfect sink behavior and climb rate are quantitatively reproduced.** These coefficients are also assumed proportional to the point defect mobility $L_{\eta^i}^d = \zeta_{\eta^i}^d M^d$ to ensure numerical stability [21]. So for all our simulations, the dimensionless form of $\zeta_{\eta^i}^d$ was set to 100 for both PDs. We assume there is no production bias, i.e. $K_0^I = K_0^V = K_0 = 1.3 \times 10^{-7} \text{dpa.s}^{-1}$, which corresponds to typical values for neutron irradiation. **For a value of $d_{\text{rec}} = 0.994 \text{ nm}$ [18] and the sink densi-**

ties adopted in our simulations, supplementary calculations not reproduced in this paper for brevity show that the effect of recombination is negligible (kinetic regime dominated by the PD absorption by sinks). The simulations are performed for the usual glide system (001)[100] in bcc crystals. All these parameters have been chosen to reproduce the experimental conditions given in [23], one of the scarce studies characterizing chemical segregation around dislocations and grain boundaries under irradiation. Moreover, in this study, segregation measurements were performed on Fe–Cr model alloys of ferritic–martensitic steels, for which the presence of other alloying elements than Cr is very limited. Then, it is reasonable to compare these experimental results with simulations where only Fe and Cr are considered.

b	0.283 nm
dislocation core energy	80 eV.nm ⁻¹
dislocation core width	2.264 nm
PF cell size a_0	0.283 nm
N1	64
N2	128
domain size	36.2 × 18.1 nm ²
initial half-distance of the dipole R_0	4.528 nm
C_{11}, C_{12}, C_{44}	243, 145, 116 GPa [46, 47]
$\Omega_{\text{I}}^{\text{ref}}, \Omega_{\text{V}}^{\text{ref}}$	1.08V _{at} , -0.048V _{at} [45]
Ω_{Cr}	0
V_{at}	1.13 × 10 ⁻²⁹ m ³

Table 1: Physical parameters of the reference case.

3.2. Effect of the overall sink strength $k_{s,d}^2$ on RIS profiles at dislocations

The value of $k_{s,d}^2$ strongly depends on the studied microstructure (dislocation forests, density of dislocation loops or cavities, ...) and even for a given

microstructure, it is difficult to estimate it precisely due to the diversity of the extended defects interacting with each other. As a consequence, a parametric study is performed. First, we assume that $k_{s,i}^2 = k_{s,v}^2 = k_s^2$ and that the overall sink strength varies between 2×10^{15} and 10^{17} m^{-2} , this variation range being quite realistic [27]. The climb velocity v_{η^l} of the dislocations, defined as $\frac{\partial R}{\partial t}$ where R is the half-distance of the dipole, can be deduced from the PF outputs by the following relation:

$$v_{\eta^l} = \frac{V}{2a_0^2} \frac{\partial \bar{\eta}^l}{\partial t} = \frac{V}{2a_0^2} \frac{1}{X^*} \text{sign}(l) \left(\frac{\partial \bar{\eta}_i^l}{\partial t} - \frac{\partial \bar{\eta}_v^l}{\partial t} \right) \quad (16)$$

where the symbol $\bar{\phi}$ stands for the average value of the order parameter ϕ . The first equality is demonstrated in the Supplemental Materials and the second equality is easily derived from Eq. 3. $\frac{\partial \bar{\eta}_i^l}{\partial t}$ and $\frac{\partial \bar{\eta}_v^l}{\partial t}$ are calculated by Eq. 13 of the PF model. The values adopted for k_s^2 lead to reasonable climb velocities between 10^{-14} and $6 \times 10^{-14} \text{ m.s}^{-1}$ as represented in Fig. 2. We can also observe that the curve representing v_{η^l} as a function of k_s^2 is not monotonous: v_{η^l} increases for low values of k_s^2 , reaches a maximum and decreases at larger values of k_s^2 .

In order to understand and validate this particular variation, we compare the PF climb velocities with the ones obtained with an analytical solution established in the following. First, the following relation for the climb velocity can be deduced from Eq. 12, as shown in the Supplementary Materials:

$$v_{\eta^l} = \frac{VK_0}{2X^*a_0^2} \text{sign}(l) \left[\frac{k_s^2}{k_{\text{dislo},v}^2 + k_s^2} - \frac{k_s^2}{k_{\text{dislo},i}^2 + k_s^2} \right] \quad (17)$$

In which $k_{\text{dislo},d}^2$ is the sink strength of the dislocation defined by Eq. S8, i.e. by the ratio between the quantity of PDs absorbed by the core

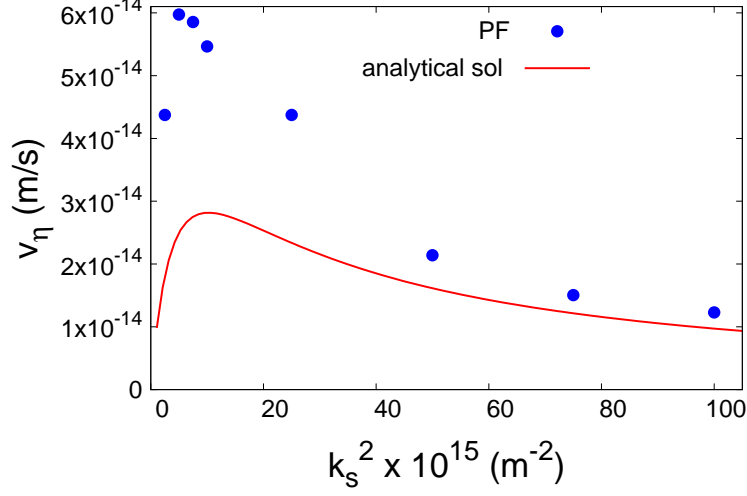


Figure 2: Climb rate as a function of the overall sink strength k_s^2 associated to the surrounding microstructure. The analytical solution is given by Eq. 17.

$\frac{\partial \bar{\eta}_d}{\partial t}$ and $D^d(\bar{X}_d - X_d^{\text{dislo}})$ when the domain is irradiated at a uniform rate K_0 . Secondly, an analytical expression of $k_{\text{dislo},d}^2$ taking into account elastic effects is given by the model of Rauh and Simon [48], which considers the dislocation as a cylinder of radius r_0 and a particular boundary condition to the calculation domain described as a cylindrical reservoir of radius R : it sets the PD composition X_d to a particular value $X_d(R)$ at its surface. After calculating the amount of PDs absorbed by the dislocation $J_{\text{dislo},d}^{\text{abs}}$, the Rauh and Simon model deduces the value of $k_{\text{dislo},d}^2$ from the relation:

$$J_{\text{dislo},d}^{\text{abs}} = k_{\text{dislo},d}^2 D^d(X_d(R) - X_d^{\text{dislo}}) \quad (18)$$

The resulting expression is:

$$\frac{k_{\text{dislo},d}^2}{\rho_{\text{dislo}}} = z_0(R) + 2 \sum_{n=1}^{\infty} (-1)^n z_n(R) \quad (19)$$

with

$$z_n(R) = \frac{2\pi I_n(L/2r_0)I_n(L/2R)}{I_n(L/2r_0)K_n(L/2R) - I_n(L/2R)K_n(L/2r_0)}, \quad L = \frac{\mu b(1+\nu)\Omega_d}{3\pi(1-\nu)k_{\text{B}}T} \quad (20)$$

where ρ_{dislo} is the dislocation density, μ the shear modulus and ν the Poisson ratio. I_n and K_n are the modified Bessel functions of the n^{th} order of the first and second kind respectively. By replacing $k_{\text{dislo},d}^2$ by Eq. 19 in Eq. 17, it is possible to obtain a fully analytical expression of the climb rate as a function of k_s^2 , which is also plotted in Fig. 2.

In the regime dominated by the dislocations ($k_s^2 \ll k_{\text{dislo},V}^2, k_{\text{dislo},I}^2$), Eq. 17 tends to :

$$v_{\eta^l} = \frac{VK_0}{2X^*a_0^2} \text{sign}(l) k_s^2 \left[\frac{1}{k_{\text{dislo},V}^2} - \frac{1}{k_{\text{dislo},I}^2} \right] \quad (21)$$

The climb velocity is proportional to k_s^2 which explains the behaviour of the PF and analytical curves for low values of k_s^2 . In the opposite case of a regime dominated by the overall sink strength of the surrounding microstructure ($k_s^2 \gg k_{\text{dislo},V}^2, k_{\text{dislo},I}^2$), the expression of the climb velocity tends to zero, since $k_s^2 + k_{\text{dislo},V}^2$ and $k_s^2 + k_{\text{dislo},I}^2$ tends to k_s^2 in Eq. 17, which explains the behaviour of the curves for high values of k_s^2 . As a consequence, for intermediate values of k_s^2 , a maximum value of v_{η^l} is reached.

A closer study of the analytical expression for the climb rate in the two limiting cases $k_s^2 \gg k_{\text{dislo},d}^2$ and $k_s^2 \ll k_{\text{dislo},d}^2$ then allows to understand

at least qualitatively the non monotonous variation of both the PF and analytical curves with k_s^2 . However, the numerical results given by the PF simulations and the analytical solution are quantitatively different. This is mainly due to the fact that the model of Rauh and Simon used in the analytical solution rests in the choice of a suitable boundary condition $X_d(R)$ at the surface of the reservoir, whereas in the PF model, irradiation effects are taken into account via the creation rate K_0 . Moreover, the Rauh and Simon model expresses the quantity absorbed by the dislocation as a function of $(X(R) - X_d^{\text{dislo}})$ to deduce $k_{\text{dislo},d}^2$ (Eq. 18) whereas Eqs. 17 and S8 suppose to use $(\bar{X} - X_d^{\text{dislo}})$ instead. These different choices were shown to induce significant discrepancies in the obtained values of $k_{\text{dislo},d}^2$ [49].

In the following, we discuss Cr segregation around the dislocation as a function of k_s^2 at a given dose of 0.011 dpa. PD profiles along the axis of the dislocation dipole noted L_1 in Fig. 1 are represented on Fig. 3 and are characteristic of those observed near sinks, whether for vacancies or SIAs: their content is very low at the cores of the dislocations and exhibit more or less significant gradients in composition near them. The profiles shown correspond to a quasi-permanent regime, we notice that the more the overall sink strength of the surrounding medium increases, the more the PD average composition decreases, which is an expected result.

This fact partly explains the difference between the atomic fraction maps of Cr for the maximum ($k_s^2 = 5 \times 10^{15} \text{ m}^{-2}$) and minimum ($k_s^2 = 10^{17} \text{ m}^{-2}$) value of the climb velocity, as represented in Fig. 4. It can be seen that Cr segregation is much more spread out around the core of the dislocations in the case of the lower value of k_s^2 . Indeed, in this case, PDs are less absorbed

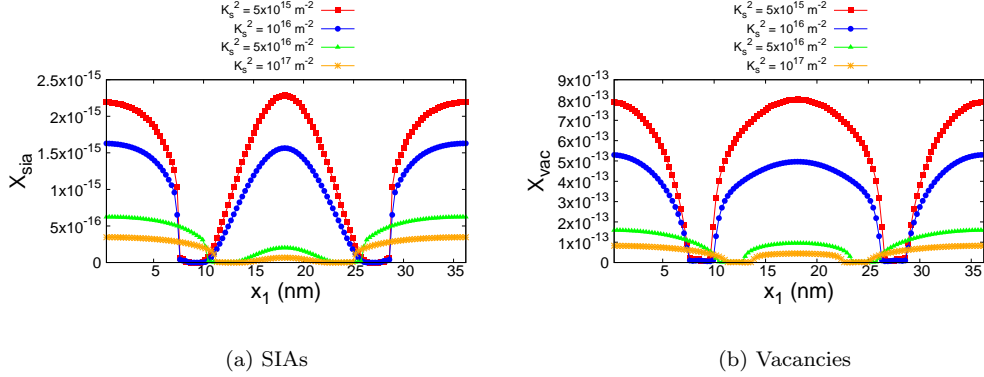


Figure 3: PD atomic fraction profiles along the dipole axis L_1 at a dose of 1.1×10^{-2} dpa.

by the surrounding matrix and then present in greater quantity around the dislocations, as already shown in Fig. 3. Cr segregation which is driven by PDs is amplified in this case and results in diffusion boundary layers of greater lengths, especially in the direction parallel to the Burgers vector as shown in Fig. 5.

Moreover, the atomic fraction maps of Cr represented in Fig. 4-a) and b) are qualitatively different. For $k_s^2 = 10^{17} \text{ m}^{-2}$, the isoconcentration curve at 6% of Cr is almost circular around the core of the dislocation and of radius lower than 1 nm whereas for $k_s^2 = 5 \times 10^{15} \text{ m}^{-2}$, it exhibits two symmetrical tails with respect to L_1 which spreads over more than 2 nm behind the core in the direction of the dislocation motion. This is related to the difference of the climb velocity: for $k_s^2 = 5 \times 10^{15} \text{ m}^{-2}$, the climb velocity is high which corresponds to a kinetic regime where dislocations move faster than the diffusion of the atoms which are left behind. For $k_s^2 = 10^{17} \text{ m}^{-2}$, the climb velocity is significantly lower which corresponds to a kinetic regime where atoms diffuse faster than the climb velocity and have then enough time

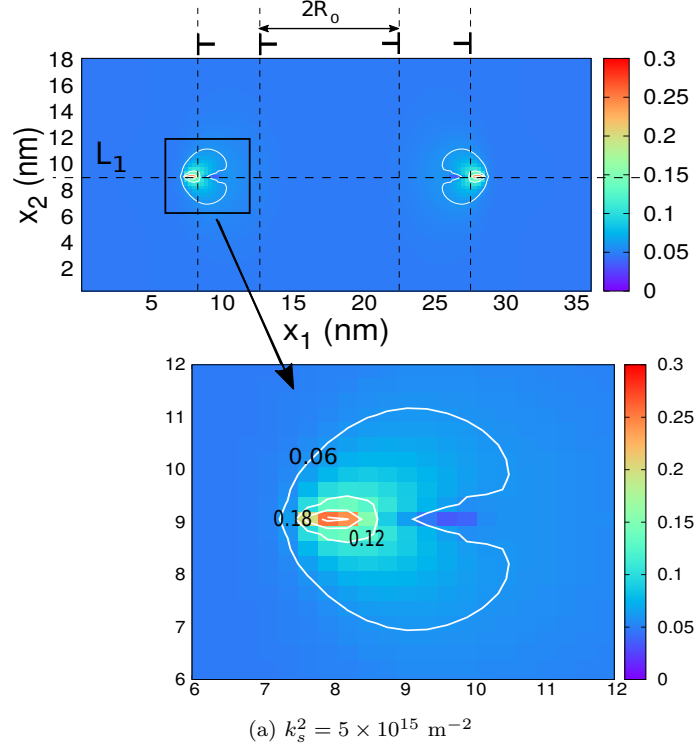


Figure 4: Cr atomic fraction maps at a dose of 1.1×10^{-2} dpa.

to follow the dislocation in its motion. In the following, the kinetic regime in which the climb rate is not negligible in comparison with the solute diffusion rate will be labeled regime I, and regime II in the opposite case.

These two distinct regimes are also visible in Fig. 6 which represents the Cr profiles along the dipole axis. For the higher values of k_s^2 (low climb rate), there is a Cr enrichment in the tension region of dislocations and Cr depletion in the compression region. fluxes of Cr atoms are coupled to the ones of PDs: Cr enrichment is due to SIAs and depletion due to vacancies [18]. Since vacancies are attracted in the compression zone of dislocations and expelled from the tension zone, while the opposite behavior is observed

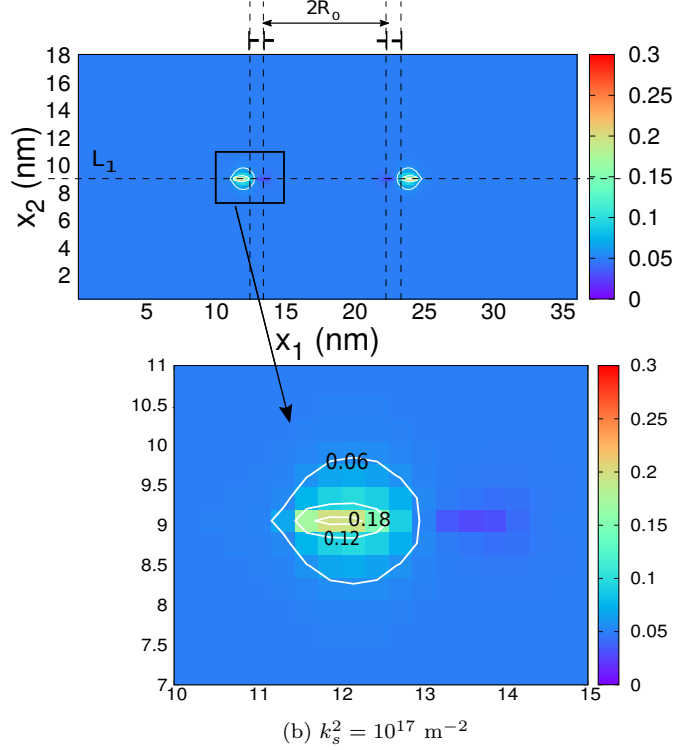


Figure 4: (Continued) Cr atomic fraction maps at a dose of 1.1×10^{-2} dpa.

for SIAs, it results in Cr enrichment in the tension region and Cr depletion in the compression region of dislocations. However, these arguments are valid only in the case where the sink moves slower than the atom diffusion, which corresponds to low climb rates. For lower values of k_s^2 (high climb rate), there is a significant change in the Cr profile with the presence of a bump in the compression region instead of a depleted zone as observed in the previous case. Plotting the Cr segregation profiles in Fig. 7 as a function of dose provides a better understanding of the establishment of these profiles. In fact, for both values of k_s^2 , there is a transition between a profile depleted in the compression region of dislocations (typical of regime II) to a profile with

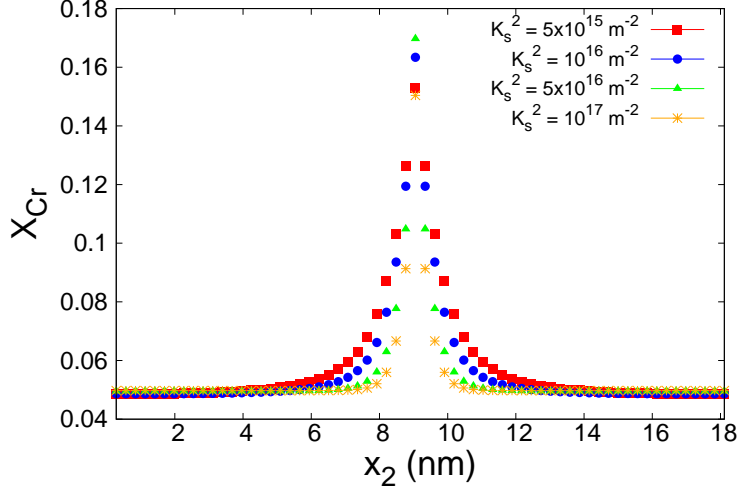


Figure 5: Cr atomic fraction profiles along the direction perpendicular to the dipole axis L_1 passing through the core of the dislocation defined as the position where $\eta^l \approx 0.5$ (dose of 1.1×10^{-2} dpa).

a bump in the compression region (regime I). During the loop growth, Cr depletion in the compression region is no longer observed or very attenuated. This can be explained by the fact that the compression region moves towards the position where the tension region was previously during the loop growth. As the tension region was initially enriched in Cr, this region will become progressively depleted in Cr in order to establish the Cr segregation profile of the compression zone. However due to the motion of dislocations, the establishment of this Cr profile in the compression region (depletion) does not have time to fully occur. Moreover, the bump appears sooner in the compression zone during the establishment of the profile in the case where the climb rate is higher, since regime I is more probable to occur in this case.

Fig. 4 shows that the peak Cr concentration is reached along L_1 . It then

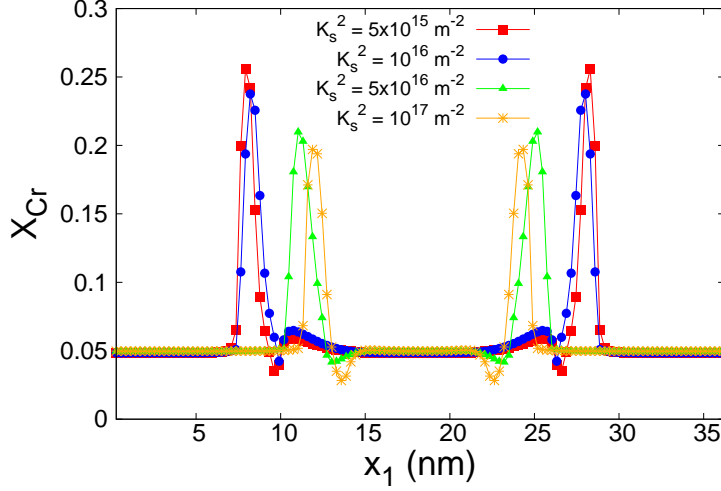


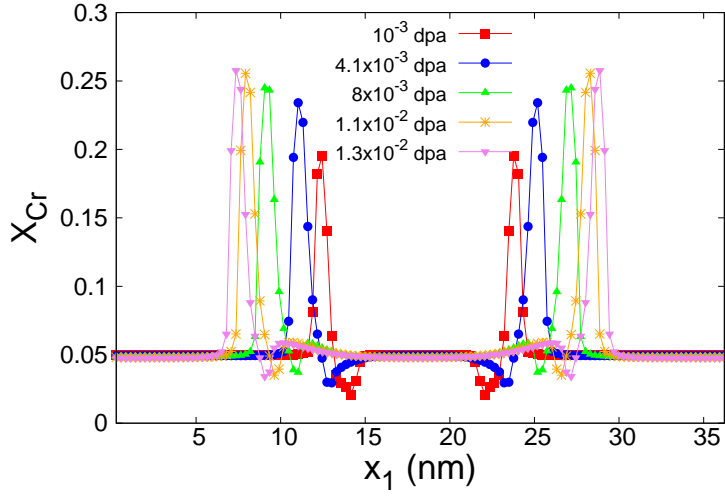
Figure 6: Cr atomic fraction profiles along the dipole axis L_1 at a dose of 1.1×10^{-2} dpa for different values of k_s^2 .

also appears on the profiles of Fig. 7: it increases slightly with the dose and is higher in the case $k_s^2 = 5 \times 10^{15} \text{ m}^{-2}$ than in the case $k_s^2 = 10^{17} \text{ m}^{-2}$, with a difference of around 3 at%. Indeed, Cr segregation is driven by PDs which are less absorbed for the lower value of k_s^2 . As a conclusion, Cr segregation is stronger at low sink strengths in terms of the spread of the profiles (Fig. 4 and 5) but also in terms of the peak Cr concentration (Fig. 6 and 7).

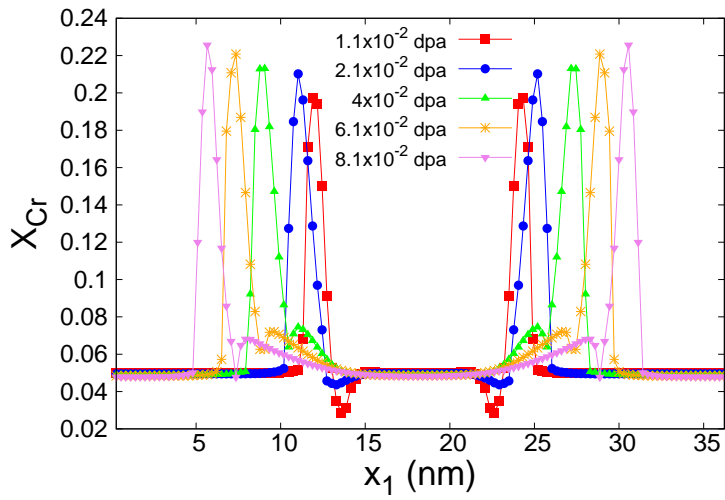
3.3. Comparison of the simulation results with experiments

In the experimental work of [23], dislocation lines were observed by APT in neutron irradiated Fe-5%Cr alloy and identified owing to segregation of Cr, Si and P. Profiles of the solute excess defined as $X_{\text{Cr}}^{\text{xcs}} = X_{\text{Cr}} - X_{\text{Cr}}^{\text{nom}}$ through two distinct dislocation lines reveal they are asymmetrical:

- (i) Cr segregation is globally clearly positive around the dislocation on a



(a) $k_s^2 = 5 \times 10^{15} \text{ m}^{-2}$



(b) $k_s^2 = 10^{17} \text{ m}^{-2}$

Figure 7: Evolution of the Cr atomic fraction profile along the dipole axis L_1 .

length of around 3 or 4 nm;

(ii) slightly depleted zones around the dislocations of around 1 at% with respect to $X_{\text{Cr}}^{\text{nom}}$ can however be observed;

(iii) The maximum value $X_{\text{Cr}}^{\text{xcs,max}}$ of $X_{\text{Cr}}^{\text{xcs}}$ along the profile is different for the two dislocations: $X_{\text{Cr}}^{\text{xcs,max}}$ is about 23 at% as measured on the first dislocation, and 10.5 at% for the second one.

Due to the choice of the technique, precise chemical data relative to Cr segregation were obtained but some information are lacking to do a precise comparison with the numerical results reported in this paper:

(i) the glide system and the nature (screw or edge) of the dislocations were not determined. Rigorously, these data are needed in the model to calculate the elastic interactions between the dislocations, the solute atoms and the PDs (Eq. 9).

(ii) the Cr profiles have been measured along a direction perpendicular to the dislocation lines through the cores, but its precise orientation relative to the Burgers vector is not known. In the case of an edge dislocation, if this direction is perpendicular to the Burgers vector (L_1), the profile is asymmetrical like in Fig. 7, with a clear segregation contrast between the compression and dilatation zones. In the opposite case where this direction is parallel to the Burgers vector, the profile is symmetrical like in Fig. 5. Then, the Cr profile theoretically depends on that direction.

Concerning (ii), some indirect hints are however given in [23] to deduce the nature of the dislocation as well as the orientation of the direction along which the profile is measured. Indeed, a systematic shift is reported in the experimental profiles of about 1 nm between Si and Cr segregations in the accommodation dislocations of grain boundaries. To explain this result, the

authors assumed that these dislocations are edge and then generate a stress field with which solute atoms elastically interact: oversize (respectively undersize) atoms segregate in the dilated (respectively compressed) part of the edge dislocations. As Si atoms are undersize and Cr atoms oversize in Fe–Cr alloys, the partitioning of these species in the stress field around the dislocation could explain the shift observed between Cr and Si profiles provided that the direction profile passes through both the compression and dilatation zones like L_1 . The fact that the shifts around the successive accommodation dislocation lines are observed along a direction belonging to the plane of the grain boundary supports this hypothesis. In other words, such a shift may be considered as an evidence of two information: the dislocation is edge and the profile direction is L_1 .

Concerning the first dislocation, the same shift as in grain boundaries is observed, then suggesting that this dislocation is edge and that the Cr profile is measured along a direction close to L_1 . As a consequence, the experimental Cr profile for the first dislocation can be compared to the simulated ones, which are represented on Fig. 7: they are also along direction L_1 and obtained for an edge dislocation belonging to the glide system (001)[100], all the other parameters of the model (Cr composition, temperature, flux) corresponding to the system studied in [23].

The calculated profiles also exhibit some positively segregated zone of around 3 nm large, in good agreement with experimental observation (i). They also show a slightly depleted zone similar to (ii). Finally, the maximum values of these calculated profiles are about 26 and 23 at% for respectively $k_s^2 = 5 \times 10^{15}$ and $k_s^2 = 10^{17} \text{ m}^{-2}$, leading to a maximum Cr excess $X_{\text{Cr}}^{\text{xcs,max}}$

of 21 and 18 at%. These values are also very close to the one observed for the first dislocation. However, this is not the case for the second one. As mentioned above, these different levels of segregation may be due to the different natures or glide systems of the investigated dislocations. The comparison with the numerical results suggest that the first dislocation is edge and that the measurement direction is perpendicular to the burger vector but not for the second one. This conclusion is supported by the fact that there is no shift between the Cr and Si segregation for the second dislocation. We will come back to this point in the discussion. To conclude, there is one dislocation for which a good agreement between the simulation results and experiments is obtained, which tends to prove the completeness of the present PF approach to grasp some essential features of radiation induced segregation near dislocations.

4. Influence of the physical parameters on the RIS profiles

In this part, we study the effect of several physical parameters on Cr segregation: the slip system of the edge dislocations, the relaxation volumes of PDs and Cr and the interaction between dislocations within a STGB. This investigation should allow to identify the important parameters but also, by comparison with experiments, to deduce their relevant values.

4.1. Effect of the relaxation volumes and of the dislocation slip system

Fig. 8 shows the effect of the relaxation volumes of PDs on Cr segregation for given values of the dose and k_s^2 . In the absence of elastic interactions between PDs and dislocations ($(\Omega_i = \Omega_v = 0)$), the cores do not move. Indeed, there is no elastic absorption bias between vacancies and SIAs at disloca-

tions in this case, moreover, the surrounding microstructure is considered as an unbiased sink ($k_{s,I}^2 = k_{s,V}^2$), PDs are then attracted in the same quantity at steady state at the cores which implies no growth. We have already mentioned that the preferential attraction of SIAs and the repulsion of vacancies in the tensile region were at the origin of the strong Cr segregation in this zone. As such a dissymmetry of the PD profiles cannot be reproduced if we do not take into account their relaxation volume, the Cr profile appears as symmetrical in Fig. 8. Moreover, in this latter case, the sink is neutral and a Cr enrichment is expected from the values of the Onsager coefficients at this temperature and nominal composition, for which Cr migrates preferentially through SIAs [18]. When PD relaxation volumes are taken into account, segregation of Cr is strongly amplified by the elastic interactions between PDs and dislocations: $X_{Cr}^{xcs,max} = 5$ at% without elasticity vs. 20 at% with elasticity. It is therefore required to take into account the elastic interactions between PDs and dislocations in order to correctly reproduce the levels of segregation obtained experimentally.

In the reference case, we have chosen to adopt the experimental values from [45] for the relaxation volumes of PDs. The corresponding absolute values are lower than those obtained in pure Fe [30] from ab initio simulations performed with the VASP code and leading to relaxation volumes respectively equal to $\Omega_V^{VASP} = -0.3V_{at}$ and $\Omega_I^{VASP} = 1.86V_{at}$ for vacancies and SIAs. The Cr profile in the reference case is compared to the Cr profile obtained with the ab initio values of the PD relaxation volumes in Fig. 9. Qualitatively, the two curves have the same shape, but quantitatively, the differences are significant: segregation is much more pronounced with

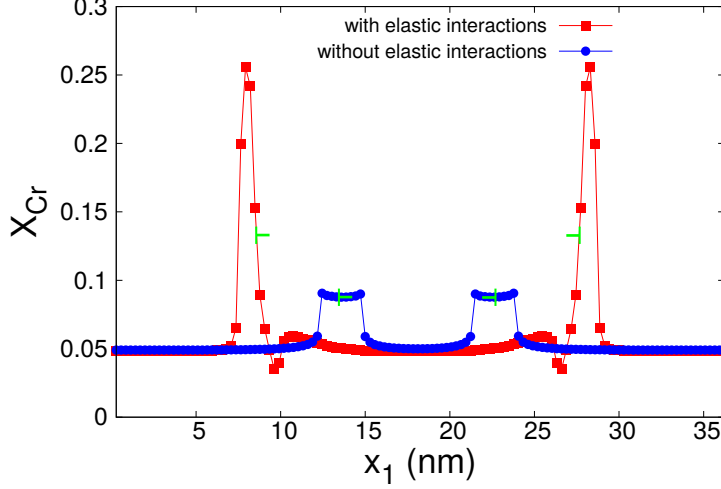


Figure 8: Cr atomic fraction profiles along the dipole axis L_1 with and without elastic interactions at a dose of 1.1×10^{-2} dpa and an overall sink strength $k_s^2 = 5 \times 10^{15} \text{ m}^{-2}$.

$X_{\text{Cr}}^{\text{max}} - X_{\text{Cr}}^{\text{min}} = 45 \text{ at\%}$ in the latter case, whereas $X_{\text{Cr}}^{\text{max}} - X_{\text{Cr}}^{\text{min}} = 21 \text{ at\%}$ in the reference case. Indeed, since $|\Omega_d^{\text{VASP}}| > |\Omega_d^{\text{ref}}|$, the elastic interactions between PDs and dislocations are amplified as well as the Cr segregation tendencies implied by them and already commented above. The effect of the PD relaxation volumes on Cr segregation is then of the first order. Moreover, a better agreement with experiment is obtained by adopting the experimental values of [45]. It can be concluded that the PD relaxation volumes are overestimated numerically in [30]. In general, it is well established that DFT methods are quite accurate in indicating the order of magnitude of point defect formation energies (to 10-15%, say) and that point defect relaxation volumes are generally overestimated (in absolute value), probably due to the limited size of the DFT simulation box used for the calculations. The results we obtained for the relaxation volume of the vacancy (roughly $-0.3 V_{\text{at}}$) are

quite standard in comparison with the values obtained for other cubic metals [30, 50]. The situation is probably the same for the relaxation volume of self-interstitials, a value that is more rarely calculated. In any case, in the spirit of our work, the values given by the ab initio calculations must be taken as plausible indicative values, and not as precise ones.

Since the lattice parameter of Cr is quite close to that of Fe, one often makes the approximation that Cr does not induce any distortion in the Fe matrix, in other words, that the relaxation volume of Cr in Fe Ω_{Cr} is null, as we assumed in the reference case. However, some studies [51] report a relaxation volume Ω_{Cr} of up to 0.06, which is not negligible. If we assume that $\Omega_{\text{Cr}} \neq 0$, it is necessary to study whether the elastic interactions between Cr atoms and dislocations can significantly influence their segregation. This type of interaction is conventionally known to be at the origin of the formation of Cottrell atmospheres, which illustrate equilibrium segregation. The value of the relaxation volume being positive according to [51], this could also explain a positive segregation of Cr in the zone in tension and negative in the zone in compression and thus amplify the trends already observed due to PD flux couplings. Fig. 9 shows small differences between the results obtained for the reference case ($\Omega_{\text{Cr}} = 0$) and for $\Omega_{\text{Cr}} = 0.06$. We can therefore deduce that if Ω_{Cr} has an influence on the Cr segregation profile, it is of the second order compared to the much larger effect of the PD relaxation volumes. In [23], the authors could not conclude on the purely thermal or irradiation-induced origin of the segregations of chemical species at grain boundaries and dislocations, since no experimental data was available before the neutron irradiation. The results of the present simulations make it pos-

sible to conclude on this point, at least for Cr, namely that the segregations observed are indeed mainly induced by irradiation.

We also consider in this part the effect of the slip system. For this purpose, we change the slip system of the reference case into $(110)[\bar{1}11]$ also usual in bcc, all the other parameters being kept unchanged. By comparing the Cr profiles in this latter case with the Cr profile of the reference case in Fig. 9, we can conclude that changing the slip system has a negligible effect.

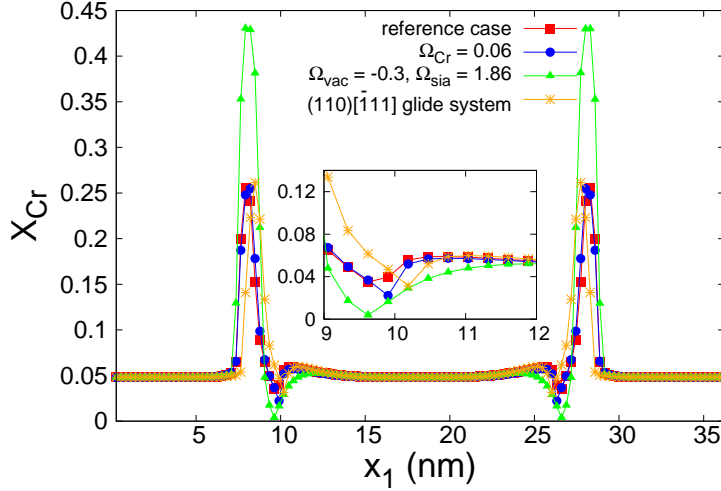


Figure 9: Cr atomic fraction profiles along L_1 at a dose of 1.1×10^{-2} dpa and for an overall sink strength of $k_s^2 = 5 \times 10^{15} \text{ m}^{-2}$.

For completeness, the climb rate is plotted as a function of k_s^2 for all the cases investigated in this section in Fig. S-1 of the Supplementary Materials.

4.2. Effect of the interaction between neighboring dislocations in a STGB

In this part are presented simulated Cr segregations in a STGB described as a stacking of edge dislocations, as represented in Fig. 1-b). The distance h

between dislocations is set at 10 nm. All the other parameters are the same as in the reference case, except $N1$ which is multiplied by 4. The simulated Cr segregation maps and profiles are given respectively in Fig. 10 and 11 for $k_s^2 = 10^{16} \text{ m}^{-2}$. In the following, we only consider the internal dislocations 2 and 3 in the stack of Fig. 1-b), the outer dislocation labeled 1 being less representative of the behavior of a dislocation inside a STGB. For the overall sink strength $k_s^2 = 10^{16} \text{ m}^{-2}$, the maximum Cr segregation excess $X_{\text{Cr}}^{\text{xcs,max}}$ in the vicinity of the dislocation cores is 15 at%, which is lower than the ones for isolated dislocations obtained in Fig. 6 and equal to 20 at% for the same dose and value of k_s^2 . Indeed, the STGB configuration in comparison with the isolated dislocation decreases the elastic field of the dislocations due to their mutual overlap, and thus the elastic bias between vacancies and SIAs the role of which has been shown to enhance Cr segregation.

The maximum Cr segregation excess $X_{\text{Cr}}^{\text{xcs,max}}$ at the grain boundaries in [23] is 7 at%, which is lower than the corresponding simulated value of 15 at%. The higher level of segregation in our simulations may be due to the difference in the distances between dislocations: 10 nm in our simulations vs. 5 nm experimentally. The same elastic argument mentioned above to explain the differences between Cr segregation in the STGB configuration and the isolated dislocation applies also here: reducing the distance between the dislocations decreases their elastic field, and thus the elastic bias between vacancies and SIAs at the origin of Cr segregation. Unfortunately, we were unable to further investigate the effect of a reduction in h . **Indeed, in this case, it is not possible to maintain the simultaneous presence of several dipoles, and only one remains, the other ones progressively disappearing.**

Each dipole is submitted to antagonist driving forces: (i) the core and elastic driving forces which tend to annihilate the dipoles to decrease the total energy of the system, (ii) the osmotic forces which tend to promote the growth of the dipoles when more SIAs are absorbed than vacancies. When h is too low, the core end elastic driving forces prevail on the osmotic forces, which may be due to the fact that the width of the dislocation in the PF model is not negligible anymore in comparison with h .

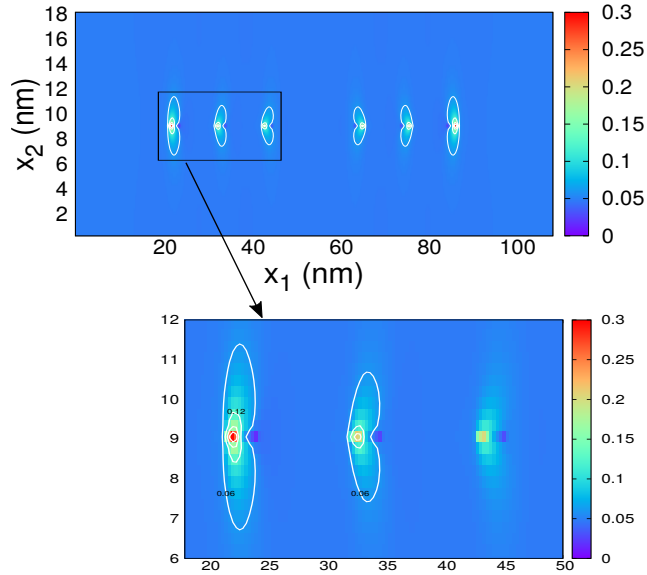


Figure 10: Cr atomic fraction map at a STGB at a dose of 1.2×10^{-2} dpa and for an overall sink strength of $k_s^2 = 10^{16} \text{ m}^{-2}$.

5. Discussion

This work has shown that with identical irradiation conditions (flux, dose), the segregation profile around the dislocation cores depends on the local environment through the mean absorption rate k_s^2 . In the situation where absorption of PDs at the cores of the dislocations is strong enough

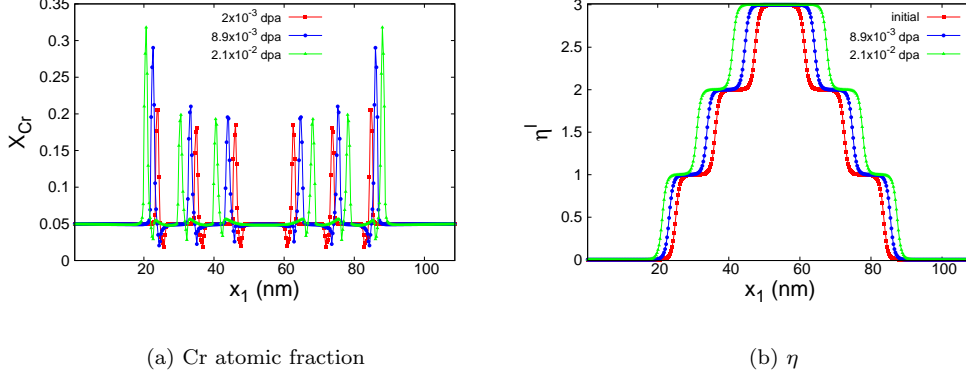


Figure 11: Evolution of the Cr atomic fraction and η^l profiles along L_1 as a function of the dose for an overall sink strength $k_s^2 = 10^{16} \text{ m}^{-2}$.

(low values of k_s^2 , see Fig. 2), we have shown for the Fe-Cr system that the climb of dislocations can be fast, inducing segregation morphologies that result from the mobility of the atoms surrounding the core being lower than that of the core of the dislocations itself. When, on the other hand, the climb is slowed by a **high mean absorption rate of the surrounding medium (high values of k_s^2)**, then the segregation profile resembles that of immobile dislocations. It should be noted that these results were obtained for an alloy for which the climb is driven by the preferential absorption of interstitial Cr atoms. The situation may be different when the segregated atoms are preferentially transported by vacancies for instance.

The effect of the Cr relaxation volume Ω_{Cr} on the RIS profile has been shown to be of the second order in comparison with the effect of flux coupling with PDs. Then, the shift observed between the experimental Cr and Si profiles in [23] can not be only explained by the attraction of undersize atoms in the compression zone and oversize atoms in the traction zone, but also by kinetic arguments. Recent ab initio calculations combined with the self-

consistent mean-field method implemented in the KINECLUE code [7] allows for the calculation of transport coefficients in ferritic Fe-X (X=Cr, Cu, Mn, Ni, P, Si) dilute alloys [8, 9]. The results show that the positive RIS of Si is mainly due to vacancy drag, which is opposite to the case of Cr. Then, in the compression zone of the dislocation where vacancies are attracted, Si segregates positively but not Cr which may explain the observed shift. If this explanation is correct, the shift still has for origin the heterogeneous stress field around the dislocation, and the conclusion about the orientation of the line along which the profiles were experimentally established holds.

In [23], a high concentration level of P is reported at the dislocation core, with an enrichment factor close to 750. However, since the relaxation volume of P is negative (P is an undersize atom in Fe), it would be expected from purely elastic argument that P segregates negatively in the traction zone and positively in the compression zone. It means that the observed P profiles can only be explained by considering the flux couplings between P and PDs. In [52], it is shown that for both vacancies and interstitials a strong binding energy is obtained with P leading to the formation of P-vacancy pairs or mixed $\langle 110 \rangle$ Fe-P dumbbells. These large interactions of phosphorus atoms with both vacancies and interstitials in the bcc Fe matrix contribute to the enrichment of P at the dislocation core [9]. The positive RIS of P certainly overcomes the elastic effect due to the relaxation volume of P previously described, as suggested by the experimental observations. This conclusion is quite similar to the one drawn for Cr, when studying the effect of the Cr relaxation volume on the segregation profile, namely that the RIS predominates over the solute relaxation volume effect.

In order to represent the whole microstructure, it is possible to treat all the sinks equivalently, namely by associating to each sink an order parameter and its evolution equation. Such an approach is tractable only if large calculation domains are considered. In order to simplify the problem, the approach used in this work to represent the microstructure is hybrid. Indeed, on one side, the dislocation dipoles are described explicitly in the domain by the order parameter η^l , which allows to track their evolution and the Cr segregation in their neighborhood. On the other side, the other sinks present in the domain are not spatially described, but their influence is taken into account through an overall and uniform sink strength in the domain. This choice is justified by the fact that only segregation in the vicinity of the dislocations has to be characterized precisely in this work, not at the level of the other sinks. In this context, the mean-field approach used to treat the other surrounding sinks turns out to be quite simple and efficient at the same time, and can be recommended when one type of extended defect should be specifically studied in comparison with the other sinks.

The RIS simulations show that due to the high level of Cr segregation reached near the dislocations, local precipitation of a new phase is expected. It would then be interesting to incorporate radiation induced precipitation in the model. The values of the elastic constants and relaxation volumes of PDs adopted in the simulations correspond to pure bcc Fe. It may be questionable since Cr composition can reach almost 30% at the cores of the dislocations in the simulations. The addition of Cr has an impact on these quantities, as shown in [53], in which PDs in bcc Fe, Cr and concentrated random Fe-Cr structures are investigated using density functional theory and theory

of elasticity in the Cr composition range between 0 and 35%. The elastic constants depend significantly on Cr composition in this range. It is also shown that the relaxation volume of a vacancy depends sensitively on whether it occupies a Fe or a Cr lattice site, whereas a unique value of the vacancy relaxation volume corresponding to Fe has been considered in our work. The relaxation volume of a SIA depends also on the nature of the dumbbell (Fe-Fe, Fe-Cr or Cr-Cr). Moreover, according to [53], the relaxation volumes of PDs differ significantly in alloys containing below and above 10% at. Cr. Future work could consist in integrating the effect of Cr on these elastic parameters to refine RIS predictions. For example, it is possible in a PF approach to consider non uniform elastic constants in the domain, this case being usually referred as heterogeneous elasticity. One way to tackle this issue is to use an iterative procedure in the Fourier space to calculate the elastic strain [35, 36, 37]. The influence on the climb rate and the RIS prediction of elastodiffusion, i.e the dependence of the Onsager coefficients with the local strain, could also be investigated. Indeed, elastodiffusion may have significant effect on the sink strength near dislocations, STGBs or interfaces [54, 55, 56, 30].

As already emphasized in the previous sections, RIS in Fe-Cr alloys is difficult to model because it results from a competition between the effect of vacancies which promotes Cr depletion and the effect of SIAs which induces Cr enrichment. Then, Cr segregation can be negative or positive, depending on the Cr composition and temperature. Moreover, in this study, the elastic interactions between the dislocations, PDs and solutes have been incorporated and turn out to have a significant impact on the resulting RIS. Finally,

a mean-field approach has been used to simulate the presence of other sinks in the surrounding environment of the dislocations. In a nutshell, due to the numerous physical phenomena included in the PF formalism used in this paper (diffusion of the PDs and the chemical species with flux coupling, dislocation climb, elastic interactions, influence of the surrounding microstructure), numerous kinetic, thermodynamic and elastic parameters must be given as inputs to the model. Due to the approximations made, uncertainties are obviously associated to these parameters which may accumulate and lead to predictions which significantly deviate from the observations. Despite these arguments, it must be mentioned that the comparison between the PF results and the experiments concerning Cr segregation at dislocations is quite satisfactory and even beyond expectations.

6. Conclusion

In this paper, a PF approach has been used in order to predict RIS at isolated dislocations or inside STGBs in Fe-5%Cr alloys. It allows to describe dislocation climb through the absorption/emission of both vacancies and SIAs as required in the context of irradiated metals. To simulate RIS, the climb model is coupled to the PD and chemical species diffusion equations in the same PF formalism. A mean-field approach is used to consider the influence of other types of microstructural defects in the domain by associating an overall and uniform representative sink strength to them. The parametrization of the model includes kinetic and thermodynamic quantities calculated at the atomic scale in previous works and elastic parameters mainly obtained experimentally. The Cr profiles simulated in this work are compared to the experimental ones obtained by APT in neutron irradiated Fe-5%Cr alloys.

For isolated dislocations, the agreement is satisfactory, considering the experimental uncertainty about the slip system and the orientation of the line used to plot the segregation profiles. Concerning STGBs, the method used to simulate them in the PF approach does not allow to numerically investigate the low experimental distances between dislocations, which may explain the discrepancy between the numerical and experimental results, even if they are of the same order of magnitude. It must be emphasized that Cr segregation is significantly affected by the climb rate in the range of realistic values investigated in this paper. With the PF method, it is possible to study separately the influence of the following physical parameters: the relaxation volumes of Cr and PDs and the nature of the slip system. This parametric study reveals that elasticity impacts RIS profiles mainly through the long-range interactions between PDs and the dislocations. As a consequence, the PDs relaxation volumes have a much higher influence on the obtained RIS profiles than the solute relaxation volume or the nature of the slip system. Despite some approximations adopted in the simulations which can be alleviated in future works, this study allows to conclude that the multiscale and multi-physics PF approach used in this paper is capable to predict RIS even in complicated configurations where the sink is biased and interacts with other microstructural defects.

7. Acknowledgements

This work was supported by the Euratom research and training programme 2015–2019 under Grant Agreement No 661913 (SOTERIA).

The authors thank the Centre de Ressources Informatiques of the université de Lille (CRI) for computational facilities.

References

- [1] H. Wiedersich, P.R. Okamoto, and N.Q. Lam. A theory of radiation-induced segregation in concentrated alloys. *Journal of Nuclear Materials*, 83:98–108, 1979.
- [2] M. Nastar and F. Soisson. Radiation-induced segregation. *Comprehensive Nuclear Materials*, 1:471–496, 2012.
- [3] L. Onsager. Reciprocal relations in irreversible processes. i. *Physical Review*, 37:405–426, 1931.
- [4] M. Nastar. A mean field theory for diffusion in a dilute multi-component alloy: a new model for the effect of solutes on self-diffusion. *Philosophical Magazine*, 85:3767–3794, 2005.
- [5] T. Garnier, M. Nastar, P. Bellon, and D. R. Trinkle. Solute drag by vacancies in body-centered cubic alloys. *Physical Review B*, 88:134201, 2013.
- [6] T. Garnier, D. R. Trinkle, M. Nastar, and P. Bellon. Quantitative modeling of solute drag by vacancies in face-centered-cubic alloys. *Physical Review B*, 89:144202, 2014.
- [7] T. Schuler, L. Messina, and M. Nastar. Kineclue: A kinetic cluster expansion code to compute transport coefficients beyond the dilute limit. *Computational Materials Science*, 172:109191, 2020.
- [8] L. Messina, M. Nastar, T. Garnier, C. Domain, and P. Olsson. Exact

- ab initio transport coefficients in bcc Fe-X (X=Cr, Cu, Mn, Ni, P, Si) dilute alloys. *Physical Review B*, 90:104203, 2014.
- [9] L. Messina, T. Schuler, M. Nastar, M.-C. Marinica, and P. Olsson. Solute diffusion by self-interstitial defects and radiation-induced segregation in ferritic Fe-X (X=Cr, Cu, Mn, Ni, P, Si) dilute alloys. *Acta Materialia*, 191:166–185, 2020.
- [10] E. Toijer, L. Messina, C. Domain, J. Vidal, C. S. Becquart, and P. Olsson. Solute-point defect interactions, coupled diffusion, and radiation-induced segregation in fcc nickel. *Physical Review Materials*, 5:013602, 2021.
- [11] A. R. Allnatt. Einstein and linear response formulae for the phenomenological coefficients for isothermal matter transport in solids. *Journal of Physics C: Solid State Physics*, 15:5605–5613, 1982.
- [12] A. R. Allnatt and E. L. Allnatt. Computer simulation of phenomenological coefficients for atom transport in a random alloy. *Philosophical Magazine A*, 49:625–635, 1984.
- [13] F. Soisson. Kinetic Monte Carlo simulations of radiation induced segregation and precipitation. *Journal of Nuclear Materials*, 349:235–250, 2006.
- [14] J. Rottler, D. J. Srolovitz, and R. Car. Kinetic Monte Carlo study of radiation-induced segregation in model metallic alloys. *Philosophical Magazine*, 87:3945–3958, 2007.

- [15] O. Senninger, E. Martinez, F. Soisson, M. Nastar, and Y. Bréchet. Atomistic simulations of the decomposition kinetics in Fe–Cr alloys: influence of magnetism. *Acta Materialia*, 73:97–106, 2014.
- [16] F. Soisson, E. Meslin, and O. Tissot. Atomistic modeling of alpha' precipitation in Fe-Cr alloys under charged particles and neutron irradiations: Effects of ballistic mixing and sink densities. *Journal of Nuclear Materials*, 508:583–594, 2018.
- [17] P. Bellon and L. Thuinet. Phase field methods. *Comprehensive Nuclear Materials 2nd edition*, 1:779–813, 2020.
- [18] J. B. Piochaud, M. Nastar, F. Soisson, L. Thuinet, and A. Legris. Atomic-based phase-field method for the modeling of radiation induced segregation in Fe–Cr. *Computational Materials Science*, 122:249–262, 2016.
- [19] L. Thuinet, M. Nastar, E. Martinez, G.F. Bouobda Moladje, A. Legris, and F. Soisson. Multiscale modeling of radiation induced segregation in iron based alloys. *Computational Materials Science*, 149:324–335, 2018.
- [20] Z. Li and D. R. Trinkle. Mesoscale modeling of vacancy-mediated Si segregation near an edge dislocation in Ni under irradiation. *Physical Review B*, 95:144107, 2017.
- [21] G. F. Bouobda Moladje, L. Thuinet, C. S. Becquart, and A. Legris. A phase field model for dislocation climb under irradiation: formalism and applications to pure bcc iron and ferritic alloys. *International Journal of Plasticity*, 134:102810, 2020.

- [22] P. Yvon and F. Carré. Structural materials challenges for advanced reactor systems. *Journal of Nuclear Materials*, 385(2):217–222, 2009.
- [23] V. Kuksenko, C. Pareige, C. Genevois, and P. Pareige. Characterisation of Cr, Si and P distribution at dislocations and grain-boundaries in neutron irradiated Fe–Cr model alloys of low purity. *Journal of Nuclear Materials*, 434:49–55, 2013.
- [24] Z. Lu, R. Faulkner, G. Was, and B. Wirth. Irradiation-induced grain boundary chromium microchemistry in high alloy ferritic steels. *Scripta Materialia*, 58:878–881, 2008.
- [25] R. Hu, G.D. Smith, and E. Marquis. Effect of grain boundary orientation on radiation induced segregation in a Fe-15.2 at.% Cr alloy. *Acta Materialia*, 61:3490–3498, 2013.
- [26] A. J. Ardell and P. Bellon. Radiation-induced solute segregation in metallic alloys. *Current Opinion in Solid State and Materials Science*, 20:115–139, 2016.
- [27] J.P. Wharry and G.S. Was. The mechanism of radiation-induced segregation in ferritic–martensitic alloys. *Acta Materialia*, 65:42–55, 2014.
- [28] O. Senninger, F. Soisson, E. Martínez, M. Nastar, C-C. Fu, and Y. Bréchet. Modeling radiation induced segregation in iron-chromium alloys. *Acta Materialia*, 103:1–11, 2016.
- [29] W. T. Read and W. Shockley. Dislocation models of crystal grain boundaries. *Physical Review*, 78:275–289, 1950.

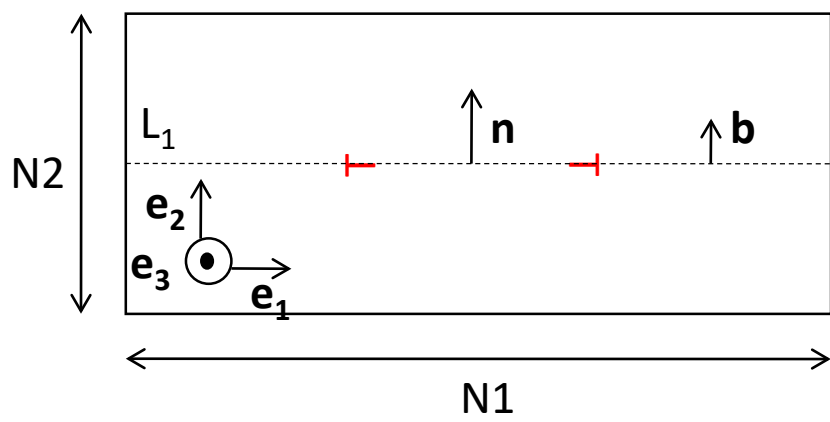
- [30] G.F. Bouobda Moladje, L. Thuinet, C. Domain, C. S. Becquart, and A. Legris. Phase-field calculations of sink strength in Al, Ni, and Fe: a detailed study of elastic effects. *Computational Materials Science*, 183:109905, 2020.
- [31] J.H. Ke, A. Boyne, Y. Wang, and C.R. Kao. Phase field microelasticity model of dislocation climb: Methodology and applications. *Acta Materialia*, 79:396–410, 2014.
- [32] P.-A. Geslin, B. Appolaire, and A. Finel. A phase field model for dislocation climb. *Applied Physics Letters*, 104:011903, 2014.
- [33] P.-A. Geslin, B. Appolaire, and A. Finel. Multiscale theory of dislocation climb. *Physical Review Letters*, 115:265501, 2015.
- [34] A. Khachaturyan. Theory of structural transformations in solids. *Wiley*, 1983.
- [35] L. Thuinet, A. De Backer, and A. Legris. Phase-field modeling of precipitate evolution dynamics in elastically inhomogeneous low-symmetry systems: Application to hydride precipitation in Zr. *Acta Materialia*, 60:5311–5321, 2012.
- [36] L. Thuinet, A. Legris, L. Zhang, and A. Ambard. Mesoscale modeling of coherent zirconium hydride precipitation under an applied stress. *Journal of Nuclear Materials*, 438:32–40, 2013.
- [37] M.-A. Louchez, L. Thuinet, R. Besson, and A. Legris. Microscopic phase-field modeling of hcp—fcc interfaces. *Computational Materials Science*, 132:62–73, 2017.

- [38] G. Oum, L. Thuinet, and A. Legris. A 3D crystal plasticity model for coherency loss during precipitation. *Modelling and Simulation in Materials Science and Engineering*, 26:065008, 2018.
- [39] T. R. Waite. Theoretical treatment of the kinetics of diffusion-limited reactions. *Physical Review*, 107:463, 1957.
- [40] M. Levesque, E. Martinez, C.-C. Fu, M. Nastar, and F. Soisson. A simple concentration dependent pair interaction model for large-scale simulations of Fe-Cr alloys. *Physical Review B*, 84:184205, 2011.
- [41] E. Martinez, O. Senninger, C.-C. Fu, and F. Soisson. Decomposition kinetics of Fe-Cr solid solutions during thermal aging. *Physical Review B*, 86:224109, 2012.
- [42] M. Nastar and F. Soisson. Atomistic modeling of phase transformations: Point-defect concentrations and the time-scale problem. *Physical Review B*, 86:220102, 2012.
- [43] A.R. Allnatt and A.B. Lidiard. Atomic transport in solids. *Cambridge University Press*, 1993.
- [44] T. Garnier, A. Finel, Y. Le Bouar, and M. Nastar. Simulation of alloy thermodynamics: From an atomic to a mesoscale hamiltonian. *Physical Review B*, 86:54103, 2012.
- [45] P. Ehrhart, K.H. Robrock, and H.R. Schober. Physics of radiation effects in crystals. *Elsevier, Amsterdam*, page 63, 1986.

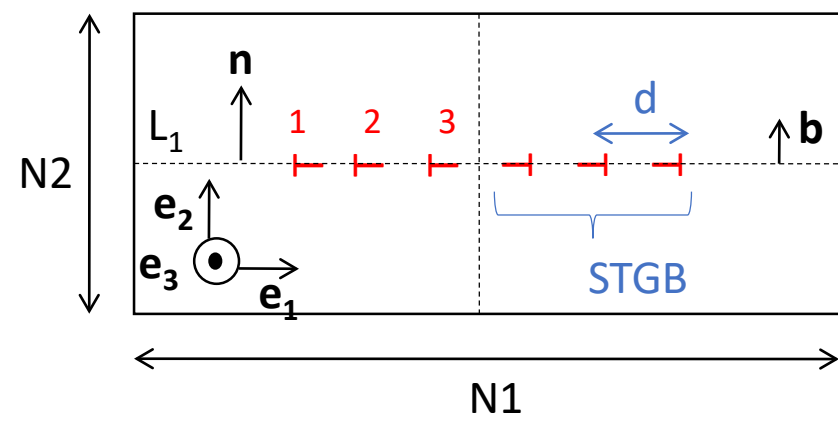
- [46] M.I. Mendeleev, S. Han, D.J. Srolovitz, G.J. Ackland, D.Y. sun, and M. Asta. Development of new interatomic potentials appropriate for crystalline and liquid iron. *Philosophical Magazine*, 83:3977–3994, 2003.
- [47] L. Malerba, M.C. Marinica, N. Anento, C. Björkas, H. Nguyen, C. Domain, F. Djurabekova, P. Olsson, K. Nordlund, A. Serra, D. Terentyev, F. Willaime, and C.S. Becquart. Comparison of empirical interatomic potentials for iron applied to radiation damage studies. *Journal of Nuclear Materials*, 406:19–38, 2010.
- [48] H. Rauh and D. Simon. On the diffusion process of point defects in the stress field of edge dislocations. *Physica Status Solidi (a)*, 42:499–510, 1978.
- [49] H. Rouchette, L. Thuinet, A. Legris, A. Ambard, and C. Domain. Quantitative phase field model for dislocation sink strength calculations. *Computational Materials Science*, 88:50–60, 2014.
- [50] D. Connétable and P. Maugis. Effect of stress on vacancy formation and diffusion in fcc systems: Comparison between DFT calculations and elasticity theory. *Acta Materialia*, 200:869–882, 2020.
- [51] I. S. Smirnov, I. S. Monakhov, E. G. Novoselova, A. L. Udovskii, and V. P. Kolotushkin. Effect of the size factor on the lattice parameter and the debye temperature of iron alloys doped with chromium or vanadium. *Russian Metallurgy*, 1:18–24, 2013.
- [52] C. Domain and C.S. Becquart. Diffusion of phosphorus in alpha-Fe: An ab initio study. *Physical Review B*, 71:214109, 2005.

- [53] J. S. Wrobel, M. R. Zemła, D. Nguyen-Manh, P. Olsson, L. Messina, C. Domain, T. Wejrzanowski, and S. L. Dudarev. Elastic dipole tensors and relaxation volumes of point defects in concentrated random magnetic Fe-Cr alloys. *Computational Materials Science*, 194:110435, 2021.
- [54] A. Vattré, T. Jourdan, H. Ding, M.-C. Marinica, and M. J. Demkowicz. Non-random walk diffusion enhances the sink strength of semicoherent interfaces. *Nature Communications*, 7:10424, 2016.
- [55] D. Carpentier, T. Jourdan, Y. L. Bouar, and M.-C. Marinica. Effect of saddle point anisotropy of point defects on their absorption by dislocations and cavities. *Acta Materialia*, 136:323–334, 2017.
- [56] T. Jourdan and A. Vattré. A continuous model including elastodiffusion for sink strength calculation of interfaces. *Computational Materials Science*, 153:473–478, 2018.

Phase-field modelling of radiation induced segregation near dislocations in Fe-Cr alloys

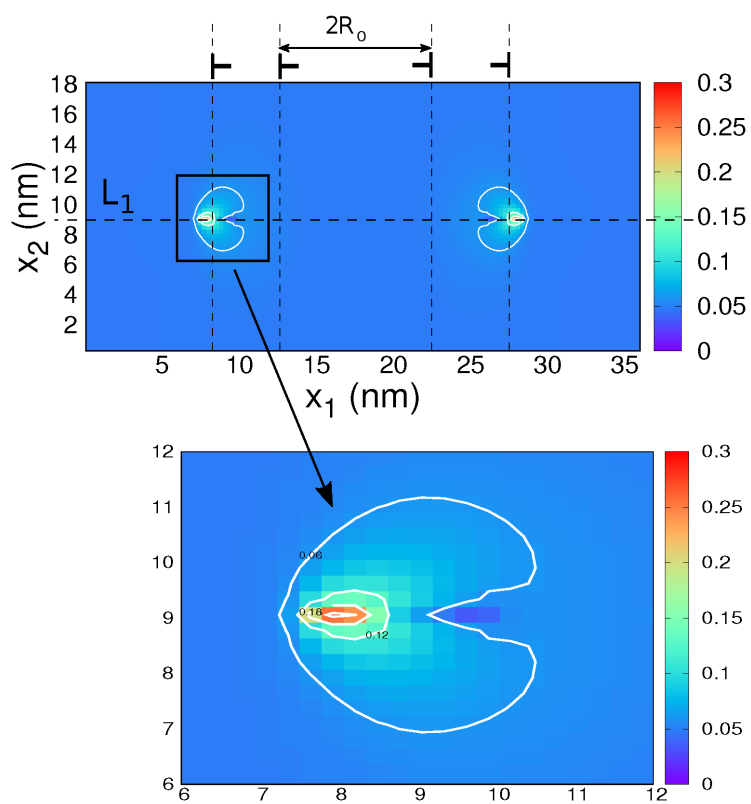


Edge dislocation dipole

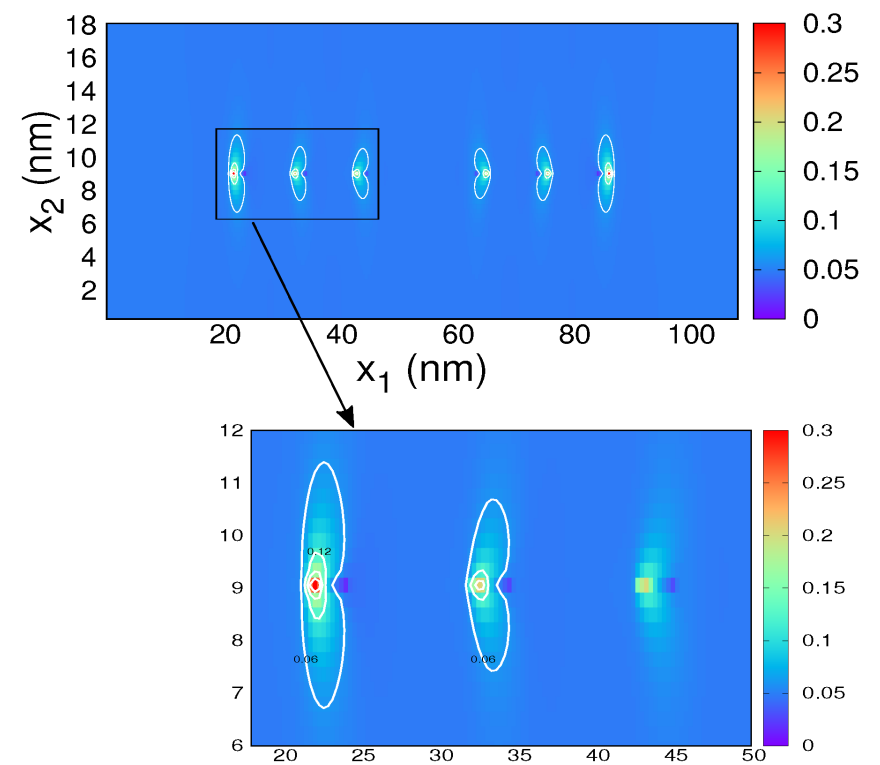


Pile-up of edge dislocation dipoles

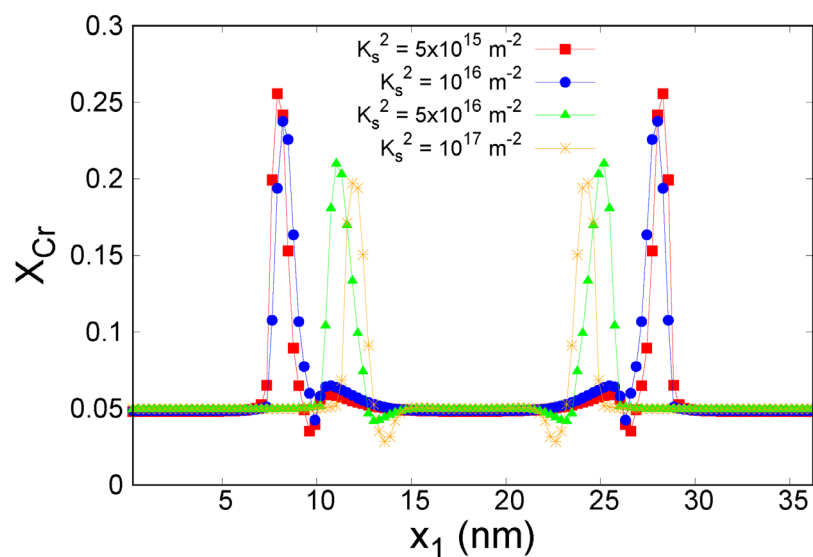
Results



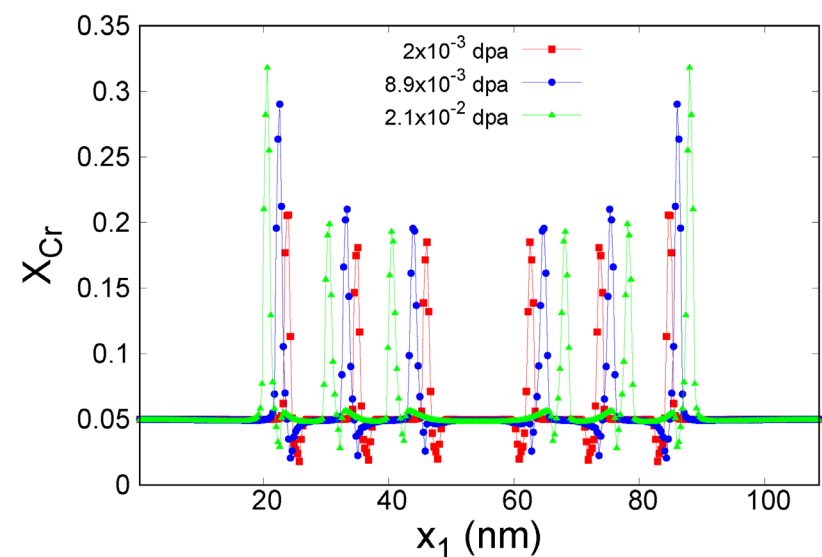
Cr atomic fraction maps at 1.1×10^{-2} dpa



Cr atomic fraction maps at 1.2×10^{-2} dpa



Cr atomic fraction profiles along L_1 at a dose of 1.1×10^{-2} dpa for different sink strengths of the surrounding microstructure



Cr atomic fraction profiles along L_1 as a function of the dose